MDPI

Article

Coherence Change-Detection with Sentinel-1 for Natural and Anthropogenic Disaster Monitoring in Urban Areas

Prosper Washaya [1], **Timo Balz** [1,2,*] and **Bahaa Mohamadi** [1]

1   State Key Laboratory of Information Engineering in Surveying, Mapping and Remote Sensing, Wuhan University, Wuhan 430072, China; pwashaya9@gmail.com (P.W.); bh.mo@whu.edu.cn (B.M.)
2   Collaborative Innovation Center for Geospatial Technology, Wuhan 430072, China
*   Correspondence: balz@whu.edu.cn; Tel.: +86-27-6877-9986

check for updates

Abstract: Rapid, reliable, and continuous information is an essential component in disaster monitoring and management. Remote sensing data could be a solution, but often cannot provide continuous data due to an absence of global coverage and weather and daylight dependency. To overcome these challenges, this study makes use of weather and day/light independent Sentinel-1 data with a global coverage to monitor localized effects of different types of disasters using the Coherence Change-Detection (CCD) technique. Coherence maps were generated from Synthetic Aperture Radar (SAR) images and used to classify areas of change and no change in six study areas. These sites are located in Syria, Puerto Rico, California, and Iran. The study areas were divided into street blocks, and the standard deviation was calculated for the coherence images for each street block over entire image stacks. The study areas were classified by land-use type to reveal the spatial variation in coherence loss after a disaster. While temporal decorrelation exhibits a general loss in coherence over time, disaster occurrence, however, indicates a significant loss in coherence after an event. The variations of each street block from the average coherence for the entire image stack, as measured by a high standard deviation after a particular disaster, is an indication of disaster induced building damage.

1. Introduction

Remote sensing data provides a solution for rapid data acquisition during disaster scenarios as well as post disaster information needed for recovery monitoring and management. High-resolution imagery is particularly well suited for identifying changes in landscapes using various change-detection techniques. Moreover, the vast array of techniques that remote sensing technology offers when used alongside Geographical Information System (GIS) software, can reduce uncertainty and serve as a catalyzing agent for analyzing and sharing information [1]. In addition, inaccessible areas can be monitored through remote sensing technologies; for example, areas affected by forest fires can be mapped and monitored, even though they may be difficult to access physically. Efforts have been made to monitor areas affected by disasters using Synthetic Aperture Radar (SAR) imagery [2–6]. These approaches, however, have not considered the globally available data products now realized by the Sentinel-1 mission. The global availability of these data permits disaster monitoring anywhere on the planet, even in areas that lack other types of remote sensing data.

This study demonstrates how changes resulting from anthropogenic and natural disasters in urban areas can be monitored using Sentinel-1 imagery and the Coherence Change-Detection (CCD)

technique. Furthermore, this study makes a quantitative comparison of CCD results from several case studies to evaluate the applicability of this approach in varying scenarios. These comparative case studies demonstrate both the efficiency and inefficiencies of remote sensing techniques. There are precedents: Gähler [7] presents remote sensing applications for numerous case studies; flooding in Germany 2013, the Nepal earthquake in 2015, forest fires in Russia 2015, and the search for the missing Malaysian aircraft in 2014. Our study presents a fresh perspective on disaster monitoring, exploring the utility of the recently introduced, globally available Sentinel-1 archive data for detection and quantitative comparison of changes resulting from different disaster scenarios.

1.1. Monitoring Disasters: Anthropogenic and Natural Disasters with Remote Sensing Imagery

In disaster management and monitoring, high-resolution satellite imagery from different dates is especially useful for change-detection [8,9]. Change-detection is defined as a process of identifying differences in the state of an object by observing the pre- and post-event data [10]. Hoque et al. [11] reviewed the various change-detection techniques suitable for the management of tropical cyclone disasters. These events often have devastating impacts on coastal areas across the world. In 2005, Hurricane Katrina wreaked havoc in New Orleans, destroyed critical infrastructure, and damaged the natural environment [12]. Monitoring the recovery of New Orleans using remote sensing techniques, showed that even 10 years after this tropical cyclone, the average vegetation in the affected areas had not fully recovered [13]. In 2017, four major hurricanes—category three or greater—were recorded in the Atlantic by September. These included Irma, Harvey, Jose, and Maria; Maria being regarded as the worst natural disaster in the history of Puerto Rico.

Also, in 2017, California experienced its worst and most expensive wildfire season on record. There were close to 9000 wildfires tearing through the state, burning 1.2 million acres of land, destroying more than 10,800 structures and killing at least 46 people. Forest fires have become a major concern in various areas worldwide. The major fires occurring in the El-Nino year of 1997/1998 burned 25 million hectares of forest area worldwide [14]. Consequently, first responders and decision makers seek to detect and monitor forest fires in a timely way. Optical imagery, such as Landsat imagery, is intuitively understood multispectral data in the visible range of the electromagnetic spectrum, and often employed in land-use classification and disaster monitoring [15]. Landsat imagery has been successfully used to measure fire-induced deforestation and produce burned area maps [15] that support decision-making processes.

Since 2008, the National Aeronautics and Space Administration (NASA) and the United States Geological Survey (USGS) have freely provided an archive of publicly available Landsat imagery data spanning four decades; this data has been used for various applications [16]. This rich body of archival data allows researchers to compare images from different periods to identify and extract areas of changes to understand variations in landscapes over time. Landsat imagery was used to detect urban destruction related to the Syrian conflict [16], as the archive of past images has a temporal fidelity as short as eight days, at high radiometric consistency, with excellent ortho-rectification [17]. However, optical data relies on a passive sensor and, hence, is affected by bad weather conditions; but all-day and all-weather SAR can provide useful information for disaster assessment even under bad weather conditions [3].

Synthetic Aperture Radar (SAR) imagery can detect, extract, and assess disaster-induced damage, such as the destruction caused by earthquakes. SAR is an active sensing system and can overcome the drawbacks of optical imagery [3–6]. The effects of earthquakes can be devastating and may cause significant loss of life and property damage, especially in urban regions. The 2008 Wenchuan earthquake devastated cities in Sichuan province, claiming at least 69,000 lives, and was the most destructive earthquake in China over the last 50 years [18]. In 2017, a magnitude-7.3 earthquake hit the northern border region between Iran and Iraq, the hardest hit town was Sarpol-e Zahab, about 10 miles from the Iraq border [19]. Although TerraSAR-X imagery has been used to detect and assess building damage after an earthquake, this data is sometimes not available for some areas in post-disaster

situations. The Sentinel-1 system is a SAR system that, through large-scale mapping capability and high revisiting frequency [20], provides solutions to this drawback.

The Sentinel-1 mission is seen as a potential game changer in operational SAR missions for decades to come [20]. The mission is the first of six Sentinel dedicated missions, introduced as part of the European Copernicus program under the domain of the European Space Agency. The Sentinel-1 system is currently based on a constellation of two SAR satellites (Sentinel-1A and Sentinel-1B) that have on-board C-band sensors. Sentinel-1A was launched on 3 April 2014; the second Sentinel-1 satellite, Sentinel-1B, was launched on 25 April 2016. With a 12-day revisit time, Sentinel-1 operates in four exclusive acquisition modes: Stripmap (SM), Interferometric Wide swath (IW), Extra-Wide swath (EW), and Wave (WV). The introduction of the Sentinel-1 constellation now ensures the timely availability of data through global coverage and the day and night, all-weather availability of data.

1.2. SAR Coherence and Change-Detection

This study employed data products from the Sentinel-1 SAR system with a C-band sensor. Synthetic Aperture Radar (SAR) is a coherent active microwave imaging method in remote sensing used for mapping the scattering properties of the Earth's surface [21]. Unlike down-looking optical sensors, SAR systems are side-looking in nature. This side-looking attribute is responsible for the three main effects inherent in all SAR images: shadow, layover, and foreshortening [22]. Layover occurs when tall objects are displaced towards the sensor when the signal reaches the top before the bottom. Foreshortening is a form of layover where the signal of an illuminated slope is compressed; subsequently appearing shorter in the SAR image than it is in reality. The shadow effect results when a steep slope or a vertical object, like a tall building, causes a radar shadow that appears black in an image. Besides the geometry, SAR signals are affected by a target object, specifically, the dielectric constant and surface roughness and the incident angle of these objects [23]. Buildings are usually structures with rectangular corners made of concrete, stone, metal, and glass where the signal may bounce from the ground to the façade then back to the sensor or from the façade to the ground and back to the sensor. Because of this so-called double-bounce effect, buildings and general infrastructure often appear bright in SAR images, and, therefore, urban built areas are usually represented by bright pixels [24]. Consequently, this study focuses on urban, built-up areas as case studies as they can be detected easily in SAR imagery.

Unlike other SAR techniques that rely on information from a single image, Interferometric Synthetic Aperture Radar (InSAR) exploits the phase differences of at least two complex-valued SAR images acquired from different orbit positions and/or at different times [21]. In addition, unlike SAR, which utilizes the amplitude information of a complex SAR signal, InSAR utilizes phase information. This phase information is used for interferometric products, like coherence images, and permits measurements of change between two images. When interferometric SAR images are not acquired simultaneously, they are affected by different types of noise: atmospheric conditions such as humidity, temperature, and pressure; and change in scatterers, for example, water body scatterers change in just milliseconds. Perpendicular baselines and volume scattering also add noise. The effect of such contributions affects both altitude and terrain deformation measurements [25]. These, therefore, influence the similarity or coherence of the phase signals.

Two waves with a phase difference that remains constant over time are said to be coherent, therefore, the higher the coherence of two waves, the easier it is to predict the properties of one of those waves given knowledge of the other [22]. In this case, coherence estimation becomes essential in generating Digital Elevation Models and measuring deformation [26,27]. Coherence is thus defined as the amplitude of the complex correlation coefficient between two SAR images [28]. The coherence is estimated on a given window size, using Equation (1) below:

$$\gamma = \left| \frac{\frac{1}{N}\Sigma_{i=0}^{N} M_i S_i^*}{\sqrt{\frac{1}{N}\Sigma_{i=0}^{N} M_i M_i^* \frac{1}{N}\Sigma_{i=0}^{N} S_i S_i^*}} \right| \tag{1}$$

where *N* is the number of neighboring pixels to be estimated, *M* and *S* are the complex master and slave images, respectively, and * denotes the complex conjugate. γ is the resulting coherence [29]. The magnitude used in the equation is so that the values of γ range from 0 (incoherent) to 1 (coherent). The coherence is only equal to 1 when *M* = *S*, which means the observation is identical in the two images because of stable objects like buildings in the scene. In reality, though, remote sensing measurements cannot be identical over time [22], as a result, values are normally below 1 and often distributed between 0.5 and 0.7, as in the case of urban built-up areas in our study. The high coherence value exhibited by built-up areas is essential as it makes them easy to identify on a coherence image. Therefore, it is essential to exploit the advantages of built-up zones in urban areas (high pixel values and high coherence values) in SAR and coherence images, taking into account the vulnerability of these areas to disasters due to population clustering.

SAR coherence has been used in various applications over the years. Prati and Rocca [30] produced coherence maps for target classification, while Bruzzone et al. [31] proposed a novel system for the classification of SAR images based on concepts of long-term coherence and backscattering temporal variability. Additionally, one well-established application of SAR is the detection of temporal changes in a scene through the Coherence Change-Detection (CCD) [32].

Coherence and intensity characteristics of SAR images have been exploited in techniques to monitor urban activities and changes. Unsupervised thresholding techniques for change-detection using the coherence and intensity characteristics of SAR imagery have been proposed in previous studies [33]. Jendryke et al. [34] combined social media messages with SAR images to express human activities and urban changes in Shanghai. The coherence characteristics of SAR images identified urban areas and the changes occurring therein; linking these data to social media messages permitted the identification of human activity occurring in those areas. However, the SAR coherence techniques applied in these studies face the following setbacks: false positives resulting from the low coherence of vegetation and water bodies and unavailability of post-disaster data.

This study, therefore, sets to solve these problems by using Sentinel-1 imagery, which is globally available, to calculate coherence before and after a disaster and improve the overall accuracy and reduce false positives by calculating the standard deviation of coherence over time and aggregate this into street blocks. Further, the study uses land use classes to measure coherence loss over time and after a disaster.

2. Materials and Methods

2.1. Data Used

Sentinel-1 C band data with VV polarization and baselines of <100 days (temporal) and <150 m (perpendicular) between master and slave images for the six study areas (Aleppo, Damascus, Raqqa, Sarpol Zahab, Santa Rosa, and San Juan) were processed using the SarProZ software [35] for coherence map generation. For Aleppo, 18 Sentinel-1 SLC images were selected. We selected one image as the master image and co-registered it to subsequent slave images, with an image baseline separation of <250 days (temporal) and <100 m perpendicular, and eight coherence maps were generated. The same technique was applied to the other study areas with variations only in the number of images used, the temporal and perpendicular baselines, and the coherence maps generated. For Damascus, 14 images were selected and 13 coherence images produced. For Raqqa, 17 images were selected and 12 coherence maps generated. In the study areas affected by natural disasters, 15 images were selected for Sarpol Zahab and 14 coherence maps generated, for San Juan, Puerto Rico, 13 images were selected and 12 coherence maps generated, and for Santa Rosa, 21 images were selected and 20 coherence maps were generated. The coherence images were integrated to street blocks and land use class polygons.

In this study, the street block was taken as the smallest element in an urban area surrounded by a road at any level of the road hierarchy. Street blocks were generated based on Open Street Map

(OSM) data, which is a form of volunteered geographic information [36]. Street blocks may vary in size, for example, from a block of a few residential apartments to a whole university campus.

Landsat-5 and Landsat-8 images were classified using the supervised classification technique and built-up, vegetated, water bodies, and bare soil were identified as the land-use types in the six study areas using ENVI Software (ENVI, Melbourne, FL, USA). Classification of the optical imagery distinguishes classes in the study areas and permits analysis of the ways in which different disasters affected coherence in the different areas.

2.2. Workflow

The methodology is divided into two parts, which can be broadly categorized as image processing and image analysis (refer to Figure 1). The image processing involves coherence image generation to identify areas and the changes that have taken place therein. The process of coherence map generation included the following steps: image stacking, slave and master selection and extraction, sub-setting the study area, downloading the external Digital Elevation Model (DEM), image filtering, interferogram generation, coherence map generation, and exporting the orthorectified coherence maps in TIFF format. The coherence images were then classified into areas of change and no-change. ArcGIS/ArcMAP software (ArcGIS 10.5, Redlands, CA, USA) was used to perform this task. The images were divided into two classes, and a threshold of 0.6 was applied. The threshold can be calculated using the Renyi's entropy to convert the image into a binary image showing areas of change and no change [33]. However, for urban areas, the 0.6 threshold is considered optimal when identifying built up areas in coherence images [24]. This threshold may vary when longer temporal baselines are considered and also depends on regional factors. In our study, areas with a coherence below the threshold were considered as changed areas and those above were considered as unchanged areas. The results are threshold-based maps classified into change (0) and no change (1) areas.

The study areas were extracted from the coherence images using the shape files to mask out the study area, this was done in order for us to focus on the urban area of the affected regions. The resulting masked coherence images were then converted into point data. This was done to enable the integration of the coherence values to street blocks, which are polygons. The point data was then integrated into the street blocks and the average coherence value per street block was calculated for each image. Standard deviation was then calculated to show which street block deviated from the average over time, indicating change. Standard deviation is, however, not a measure of instability, but a measure of change. For example, coherence in vegetation exhibits instability due to constant de-correlation but has a low standard deviation. A sudden change in a building, however, will result in a high standard deviation as this will show a huge shift from the norm; thus, indicating a change in coherence for buildings. Other types of polygons, for example, grids or hexagons, can be used for this purpose; however, street blocks are more appropriate in an urban set-up as they are relatable objects in the real world [34]. The same technique was applied to the classified polygons by joining them to the coherence point data and calculating the average coherence over time.

To make a comparison of the change-detection results for the different disasters, we extracted the built-up area and vegetation from the land-use classes (a built-up area is less sensitive to coherence loss, thus indicating the coherence loss resulting from a disaster). After calculating the average coherence for the urban classes in the coherence image immediately before a disaster and the image immediately after a disaster, we applied the following change-detection formulae [37]:

$$A = \frac{(T1 - T2)}{T2} * 100\% \tag{2}$$

where A is the percentage of change, $T1$ is the average coherence for the coherence image before the disaster, $T2$ is the average coherence of the image after the disaster, and A is the percentage of change.
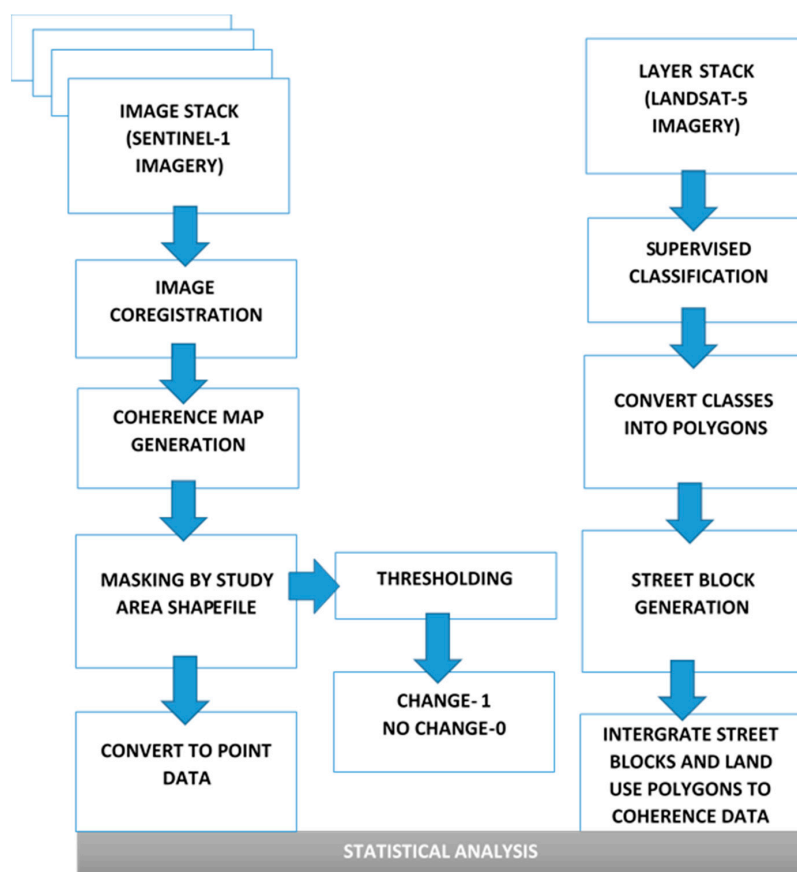
Figure 1. Methodology workflow.

2.3. Study Areas

The study focuses on the following areas affected by different types of disasters (both natural and anthropogenic). For the natural disasters, we selected San Juan, Sarpol Zahab, and Santa Rosa (San Juan) as shown in Figure 2. On 20 September 2017, Hurricane Maria struck Puerto Rico and caused catastrophic damage, which triggered a major humanitarian crisis in San Juan, the capital, and most populous municipality of Puerto Rico. In November 2017, an earthquake measuring 7.3 in magnitude devastated the Iran-Iraq border. It was the strongest on record in the region since 1967. The damage was extensive, and one of the most affected cities was Sarpol Zahab. Another notable natural disaster was the Tubbes fire of October 2017; the fire caused damage estimated at $1.2 billion US dollars, with five percent of Santa Rosa's housing stock destroyed [38].

For anthropogenic disasters, we selected the Civil War in Syria, (focusing on Aleppo, Damascus, and Raqqa) sparked by demonstrations motivated by demands for democratic reforms and release of political prisoners. The Syrian government's response escalated the tensions, which led to the demonstration shifting from their original demands to a demand for the removal of the Assad government [39]; the result was death and destruction in the country's big cities like Aleppo, Raqqa, and Damascus. In 2016, the Syrian Government embarked on a campaign to take back Aleppo city that was in the hands of the Rebels, which resulted in the devastation of the city. In Damascus, war intensified in July 2012 but did not last long as the city became a Syrian government stronghold and witnessed isolated cases of rebel attacks and suicide bombings. In Raqqa, the United States-backed Syrian Defense forces launched an operation in October 2017, which left 80% of the city uninhabitable [39].

(**a**)
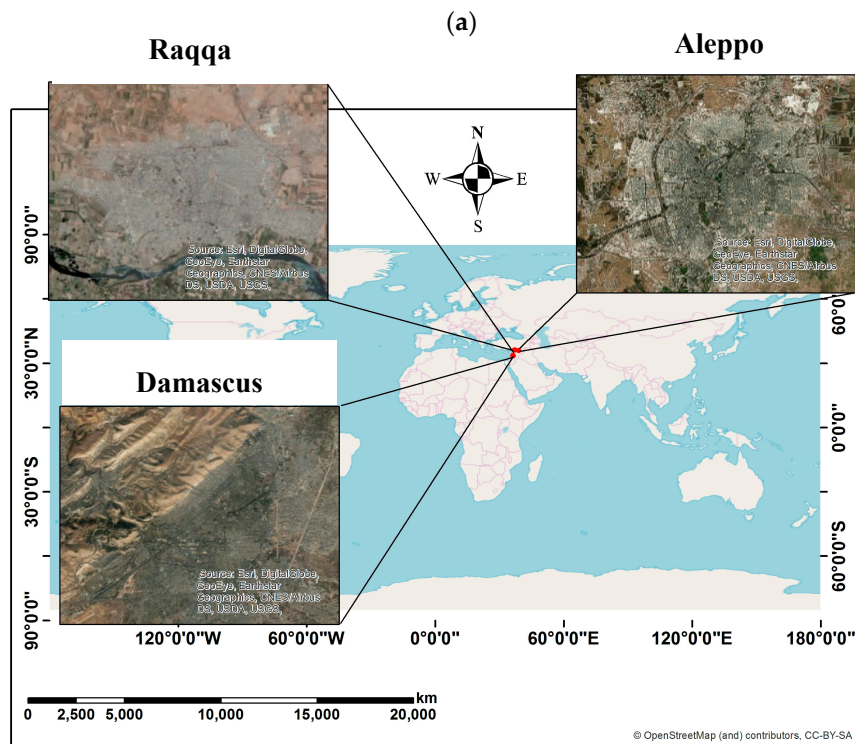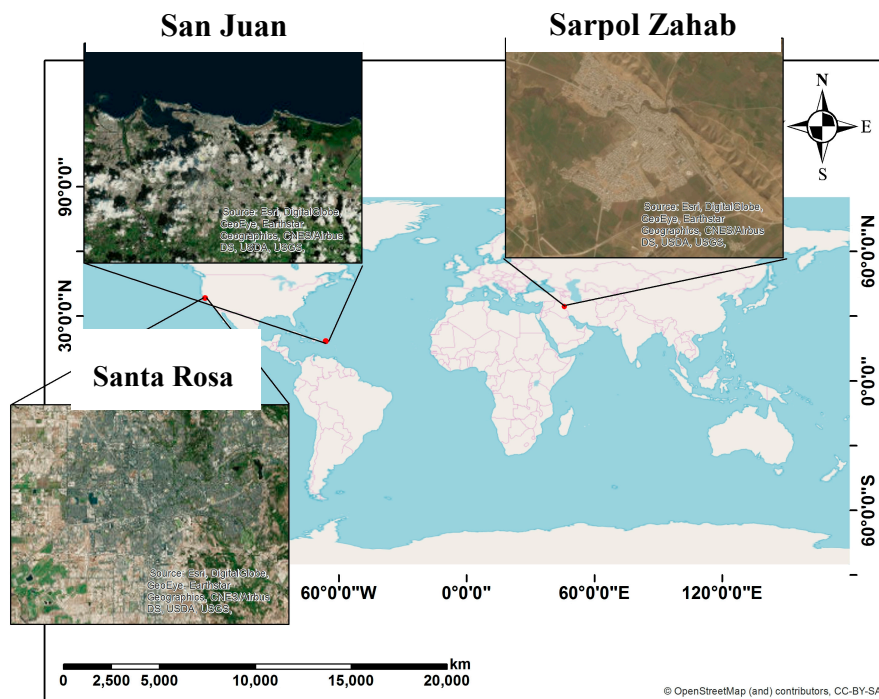
(**b**)

Figure 2. Study areas: (**a**) Areas affected by natural disasters; (**b**) Areas affected by anthropogenic disasters.

3. Results

3.1. Case Studies for Detecting Changes Using CCD

This section presents the results of an analysis of averaging and standard deviation values calculated from the coherence images generated to detect changes in the six study areas. In addition, the supervised classification results permitted an investigation of the response of various land-use classes to coherence loss in the face of disasters.

In general, the results exhibit loss of coherence over time. However, by selecting the image in the middle of the image stack timeline as the master image, coherence matching is done to ensure that coherence loss is distributed evenly in both temporal directions (i.e., pre-master slave images and post-master slave images). For a better visual impression on the coherence images, classification is done on the images into areas of change and no change by applying a threshold of >0.6 [24].

3.1.1. Natural Disasters

Sarpol Zahab, San Juan, and Santa Rosa results are presented in this section. The Sarpol Zahab results visualized in Figure 3 show a substantial loss of coherence in the post-disaster coherence maps compared to the pre-disaster coherence maps. The pre-disaster image immediately before the disaster event (7 November 2017) exhibits coherence loss of 37.8% in the entire area. The post-earthquake image, on the other hand, exhibits a coherence loss of 70.3%. The loss of coherence can be attributed to the destruction of infrastructure (building, roads etc.) by the earthquake, which occurred in November 2017 [40]. However, the southern part of the city also seems to be experiencing coherence loss in both pre- and post-disaster coherence maps, this can be attributed to vegetation, which is highly sensitive to coherence loss as it is constantly changing.
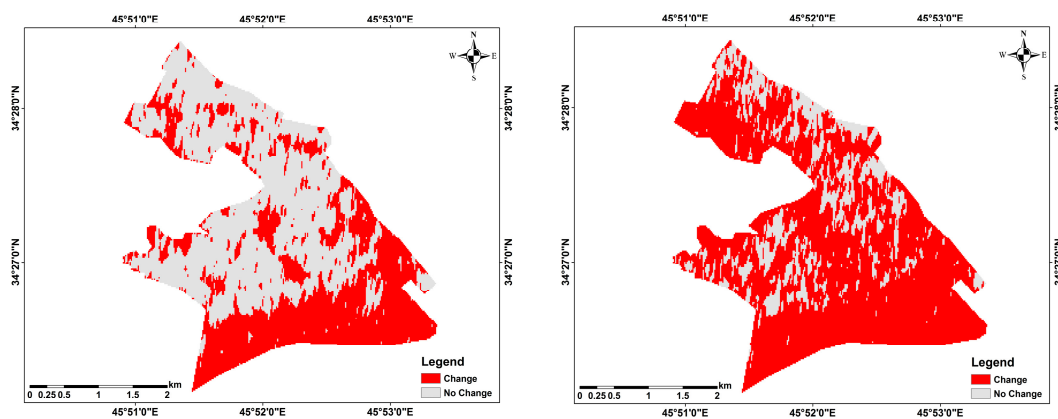

Figure 3. Sarpol Zahab coherence image classified into change and no change showing period before (7 November 2017, **left**) and after (1 December 2017, **right**) the earthquake.

In San Juan, Puerto Rico (Figure 4), results show massive decorrelation, which is an indication of hurricane-induced damages, due to the strong sensibility of interferometric coherence to water and humidity changes. For the pre-disaster coherence map, coherence loss is low but not absent, the results show areas in red (representing coherence loss) that can be attributed to lagoons, rivers, and temporal decorrelation from vegetation. The pre-hurricane coherence image (11 August 2017) shows a coherence loss of 41% while the post-hurricane coherence image (28 September 2017) shows a coherence loss of 64.4%.

In Santa Rosa (Figure 5), the post-fire disaster coherence map shows decorrelation in some parts of the city, especially in the northern part, which is the part of the city that experienced the disaster first. This may be an indication of the route taken by the fire during the disaster [41]. In the southern part, decorrelation can be seen in both pre- and post-fire disaster images. The pre-disaster image

(22 August 2017) shows that the area experienced a coherence loss of 66% while the post-fire coherence image (14 November 2017) shows that the area experienced a total coherence loss of 82%.
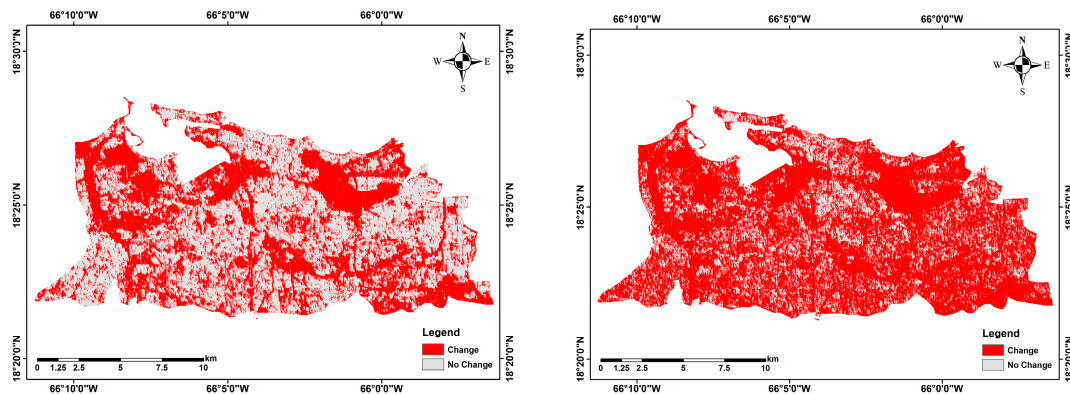

Figure 4. San Juan, Puerto Rico Coherence image classified into change and no change showing images before (11 August 2017, **left**) and after (28 September 2017, **right**) hurricane Maria.
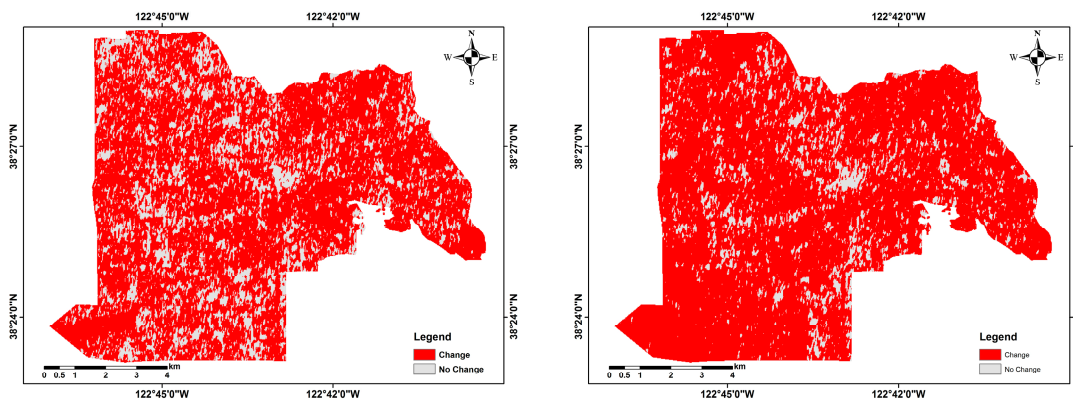

Figure 5. Santa Rosa Coherence image classified into change and no change showing images before (22 August 2017, **left**) and after (14 November 2017, **right**) the fire disaster event.

Natural disasters are usually one-time events that may occur in an area over a short period of time (minutes to hours). Wars and conflicts, on the other hand, involve a series of prolonged events occurring over many months to many years. Areas affected by the war in Syria, therefore, exhibited coherence loss differently from those affected by natural disasters.

3.1.2. Anthropogenic Disasters

For Aleppo, results show that although there was substantial coherence loss in the southeastern part of the city, in the coherence image (30 April 2017), high coherence is generally maintained in the northwestern part of the city (see Figure 6). This can be attributed to the intensification of fighting between the Syrian Government and the rebels between September and December in 2016 [42]. The coherence image (30 April 2017) is from the period after conflict intensification. It shows a 65% loss in total coherence for the city, compared to only 16% loss of coherence in the image for 4 July 2016, collected before the conflict intensified.

In Raqqa, the results in Figure 7 show a significant loss of coherence in the coherence image for 27 September 2017. This loss of coherence can be attributed to the operation launched by the U.S.-backed Syrian Democratic Forces (SDF) to capture Raqqa from the Islamic State of Iraq and Syria (ISIS) [43]. This operation lasted for several months, ending in October 2017. The coherence

image representing the period after this operation indicates a loss of 82.5% coherence. In contrast, the coherence image collected before this operation shows a 47.2 loss in coherence.
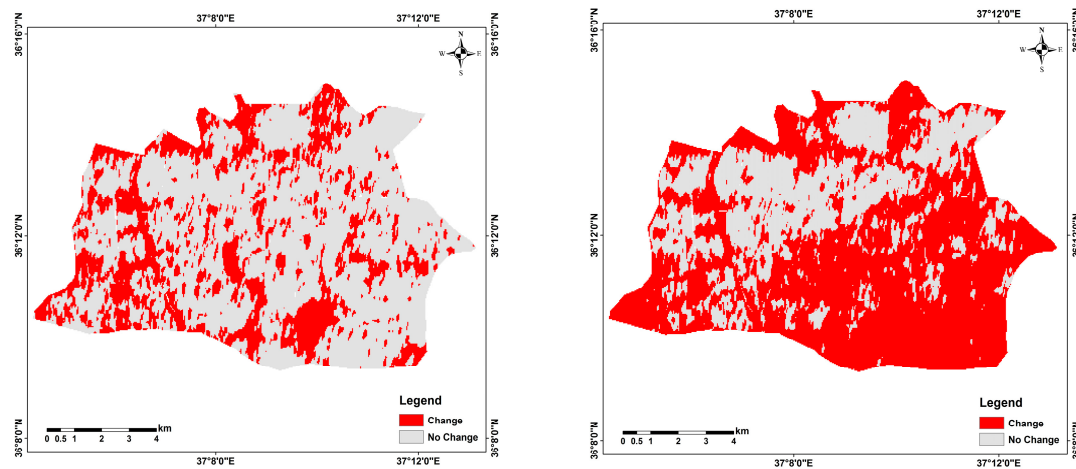

Figure 6. Aleppo Coherence image classified into change and no change showing images before and after the Syrian Government operation. Images before conflict intensification (4 July 2016, **left**) and after conflict intensification (30 April 2017, **right**).
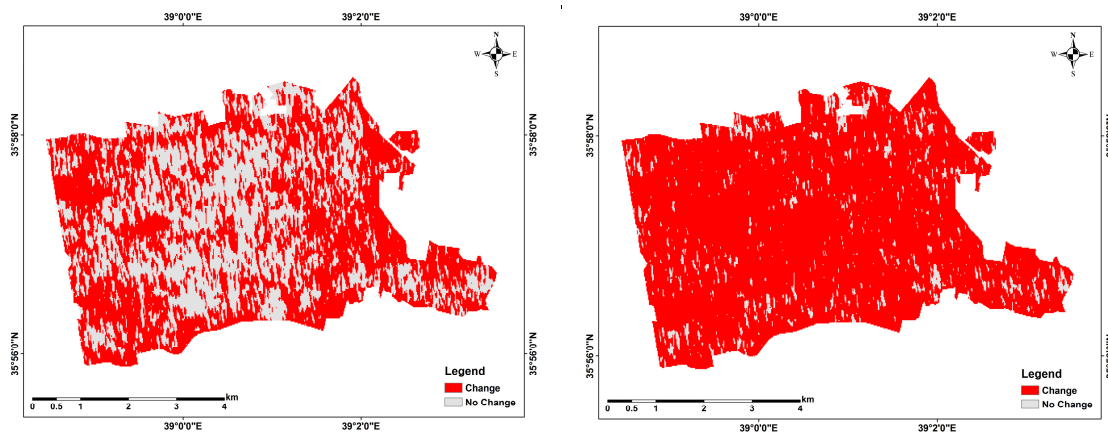

Figure 7. Raqqa Coherence image classified into change and no change showing coherence images of before (14 October 2016, **left**) and after (27 September 2017, **right**) the US-led forces operation against the Islamic State of Iraq and Syria (ISIS).

Considering Damascus, the results in Figure 8 show that towards the northeastern part of the city, a red spot is visible in both coherence maps, this area is a vegetated open space area, which is sensitive to coherence loss and is, therefore, unstable. Furthermore, coherence loss can be seen in the eastern part of the city in coherence maps on 5 April 2017 and is not visible on 31 October 2016, this movement from stability to instability can be an indication of building destruction in the area resulting from intense fighting between Syrian Government forces and rebels [44].
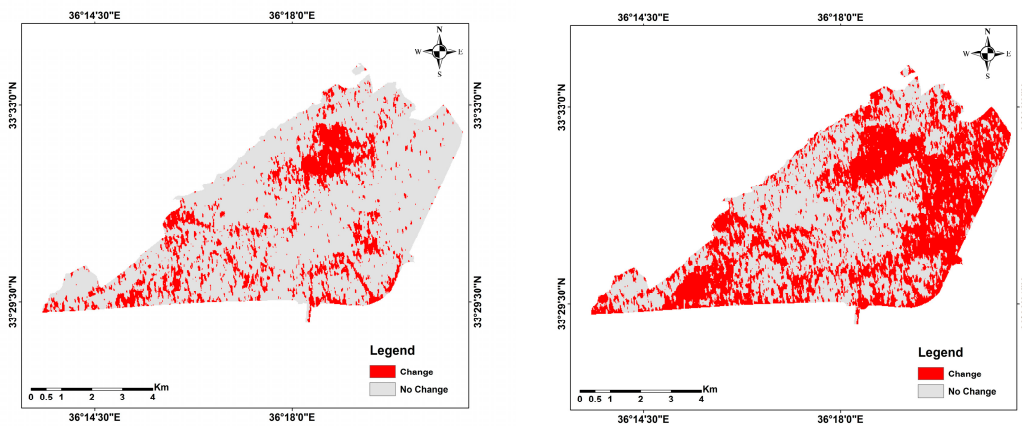
Figure 8. Damascus coherence images classified into change and no change (31 October 2016 on the **left** and 05 April 2017 on the **right**).

3.2. Analysis

3.2.1. Coherence Response to Different Land-Use Classes

Supervised classification results were used for further analysis to get an idea of how each disaster affects each land-use class.

In the study areas, areas classified as built-up, on average, show high coherence as compared to areas classified as vegetation and bare soil. Raqqa was chosen to represent the areas affected by war as it contains the most land use classes of all the war areas in the study, i.e., built-up, vegetated, and bare soil. However, there is a significant drop in built up coherence on 29 July 2017 to the extent that average coherence for the built area almost equals vegetation and bare soil (see Figure 9). This may be a direct result of the Syrian Defense Force (SDF) operation against Islamic State militants (ISIS) in the city around the same period.

For the earthquake disaster, a significant drop in coherence for all classes is observed between 7 November 2017 and 1 December 2017, which is the period after the occurrence of the earthquake. The fire disaster graph shows a dip to an average coherence of below 0.5 for all classes on 14 November 2017, which is after the fire disaster occurred, after that, average coherence remains steady for all three classes although built-up remains slightly above vegetation and bare soil. On the hurricane graph, the average coherence drops to 0.5 for built-up areas below 0.5 for vegetation and water bodies. Throughout the period, the average coherence for water bodies was under 0.5 and was only slightly affected by the hurricane as compared to vegetation and built-up areas. The average coherence increases on 10 October 2017; this could be a result of coherence recovery after floodwater evaporated weeks after the hurricane (see Figure 9).
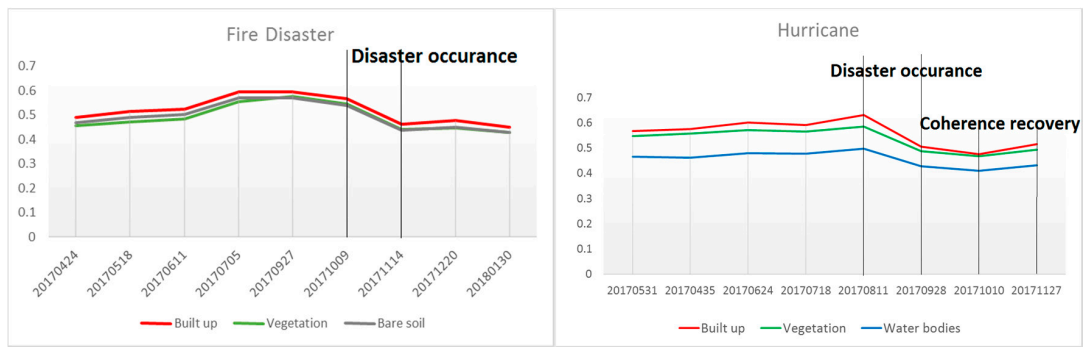

Figure 9. *Cont.*

Figure 9. Average coherence graphs for different classes for each disaster.

Comparison of Disasters

Change-detection calculated for the built-up class shows that the war in Raqqa created the highest amount of change (55%) followed by the Sarpol Zahab earthquake (40.5%), which is an indication of significant infrastructure damage. Conversely, change-detection on the built-up classes in the fire and hurricane disaster do not exhibit high levels of change, implying minimal damage on building infrastructure (with 26.4% and 22.3% respectively) as compared to the earthquake and war disasters. The vegetation class, on the other hand, was less affected by the four disasters as compared to the built-up class. In the war disaster, the vegetation class experienced a 14.3% change, in the hurricane disaster, 18% change, and fire and earthquake disasters 23% and 37% change, respectively. The results, as shown in the Figure 10 radar graph, indicate that the war and earthquake disasters have a greater impact on the built-up classes and the hurricane and fire affect the vegetation class more intensely.
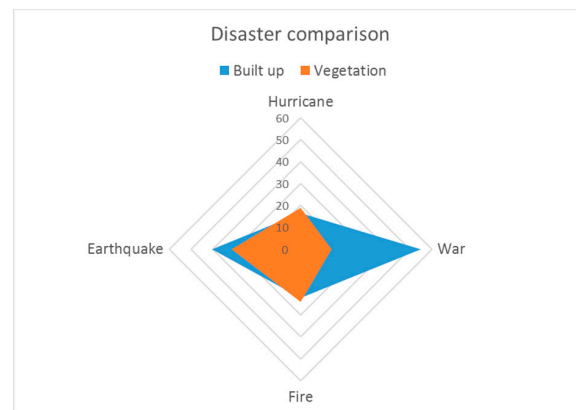

Figure 10. A comparison of built up vegetation land-use class responses to the four disasters.

3.2.2. Standard Deviation Analysis

To understand the way in which coherence in different parts of each study area responds to the various disasters and to reduce false positives from the vegetation and water bodies land use classes, we calculated the standard deviation for every street block over the study periods in the coherence maps. The standard deviation is not a measure of instability, but instead a measure of change. In the standard deviation results, the maps show changes in street blocks. Blocks with a low standard deviation are in light brown, indicating little change, while those that have experienced change (high standard deviation) are in dark brown. The study areas exhibited the following results after standard deviation calculation.

The results in Sarpol Zahab show street blocks with high standard deviation in various parts of the city. A standard deviation map of coherence images before the earthquake shows most of the

city with low standard deviation (light brown), however, a comparison with the standard deviation map of all coherence maps (pre- and post-disaster) shows that many street blocks were affected by the earthquake, especially in the northwestern part of the city (refer to Figure 11). This is verified by United Nations Institute for Training and Research (UNITR) that produced a detailed map of damaged structures and a related density map for Sarpol Zahab, seen in Figure 12 [45]. The southern part of the city shows evidence of change indicated by a high standard deviation in the map shown in Figure 11b. Satellite imagery shows this area as agriculture, and the change can be explained by change from different stages of the agricultural season, defined as planting and harvesting times.
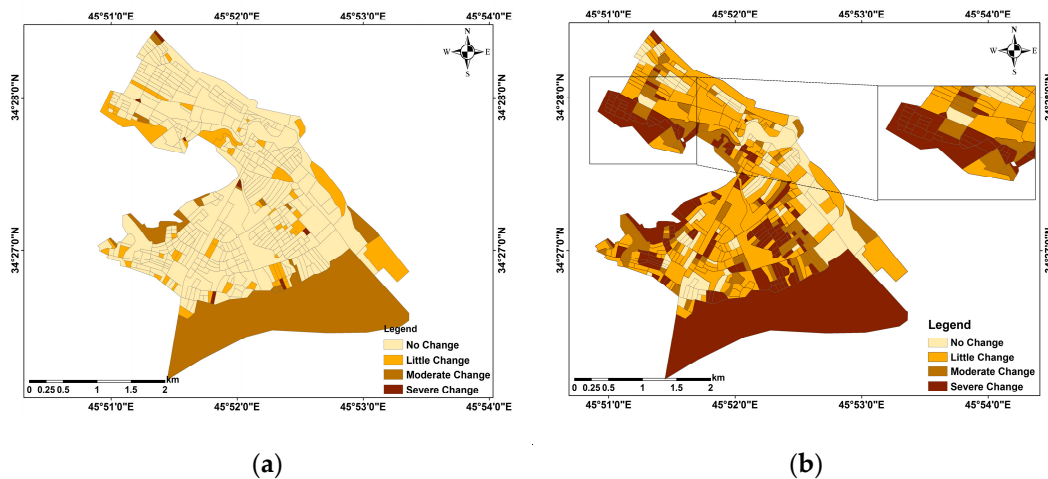

(a)   **(b)**

Figure 11. Sarpol Zahab standard deviation maps, (**a**) shows a lower standard deviation calculated with lighter colored street blocks before the earthquake disaster and (**b**) shows a higher standard deviation calculated with darker street blocks after the earthquake disaster.
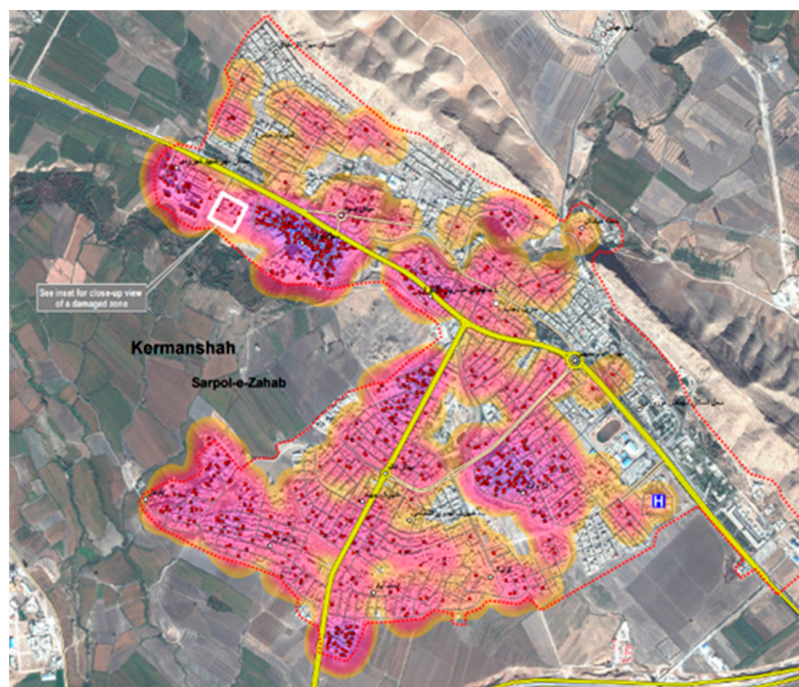

Figure 12. Damage map for Sarpol Zahab. Source: (UNITR) [45].

In San Juan, Puerto Rico, the standard deviation is high throughout the city (see Figure 13). Comparison between the pre- and post-disaster standard deviation maps shows change from light brown street blocks in the pre-disaster map to dark brown street blocks in the post disaster map. This could be an indication of the trail of disaster left by Hurricane Maria. Furthermore, it is interesting to notice that the only parts of the city showing very low standard deviations, or no change, are lagoons and water bodies. In coherence maps, these water bodies and lagoons would normally appear black all the time, indicating instability; this remains the case in the event of a Hurricane.
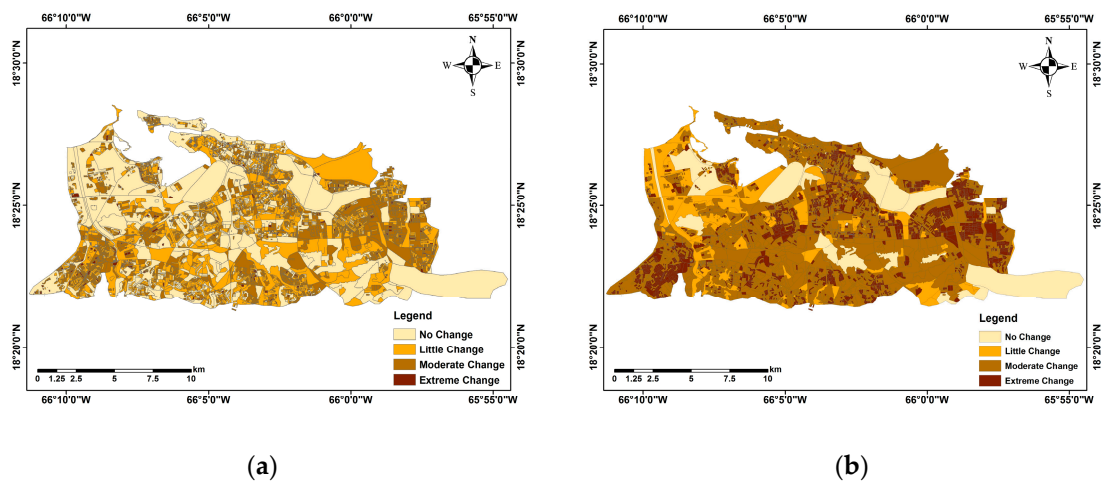

(**a**)   (**b**)

Figure 13. San Juan, Puerto Rico standard deviation map (**a**) shows lower standard deviation on street blocks before the hurricane and (**b**) shows higher standard deviation calculated after.

In Santa Rosa, California, the northern part of the city, predominantly residential, shows dark brown street blocks in the post disaster map, which implies change occurring in residential buildings. This area is Coffey Park, and media reports indicate that the fire destroyed many houses in this area [46]. This also shows that the fire came from the north of the city and destroyed houses in the north before it was contained, as shown in Figure 14. Figure 15 shows the fire route according to the New York times.
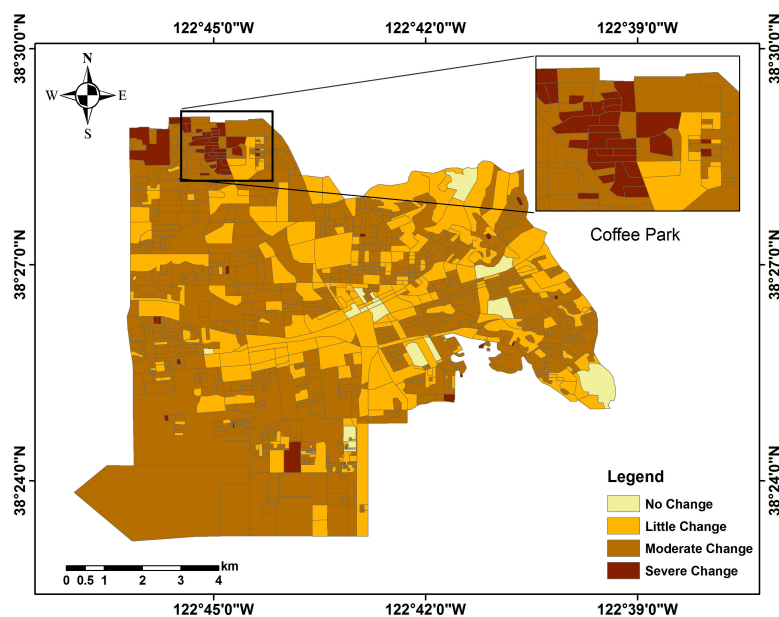

Figure 14. Santa Rosa standard deviation map indicating lower standard deviations on some street blocks in the north before the fire.
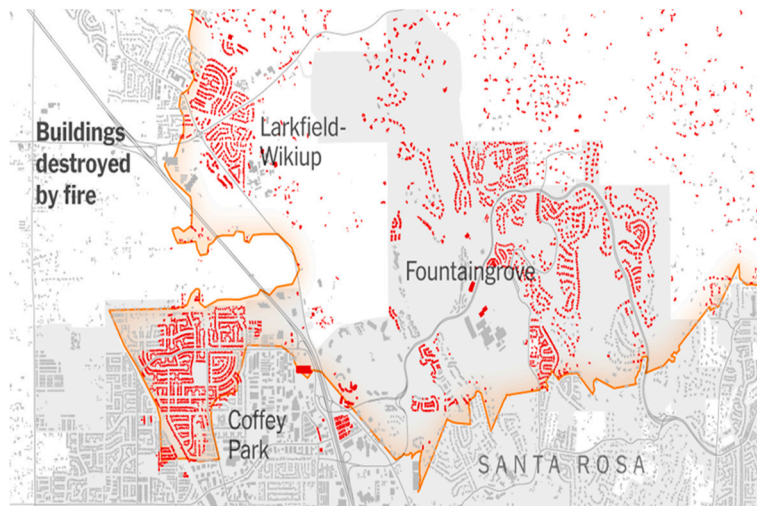
Figure 15. Santa Rosa fire route. Source: New York Times [46].

For areas affected by war, the standard deviation represents changes that occurred at different points in time on different street blocks. This means that the dark brown colors on street blocks represent changes, captured as snapshots of conflict-induced building damages, resulting from airstrikes, suicide bombings, barrel bombings, etc.

In the standard deviation map of Aleppo, the results show that street blocks located at the western side of the city exhibit a low standard deviation (light brown color), an indicator of little to no change. The eastern part of the city, however, shows a high standard deviation showing moderate to extreme change, which may be an indication of building destruction during the war. Maps from the Aljazeera news agency hint this by showing maps of the Syrian government moving to control the eastern part of Aleppo (see Figure 16). The maps show how control of the city in the eastern part changed from rebel to government control, this change indicates that conflict occurred as the government took over from the rebels. Therefore, conflict induced damages resulted in changes in these areas, hence a high standard deviation. A sample of street blocks from Karm Al-Myassar, affected by the civil conflict in the city [47], is shown in the standard deviation map in Figure 17.
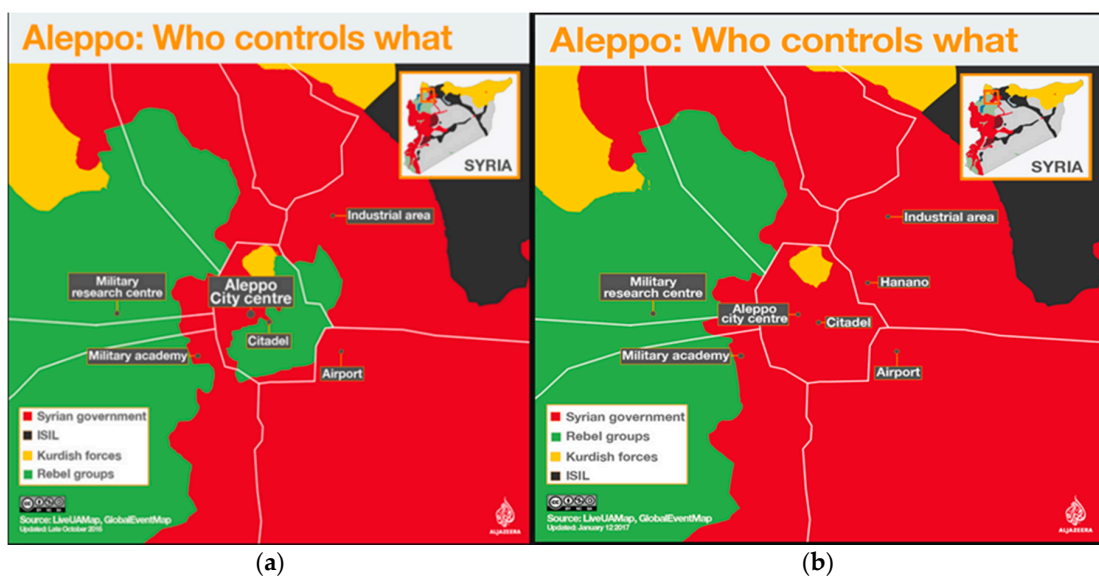

(**a**) (**b**)

Figure 16. Aleppo Territories. Before Government offensive (**a**) and after Government offensive (**b**). Source: Aljazeera [47].
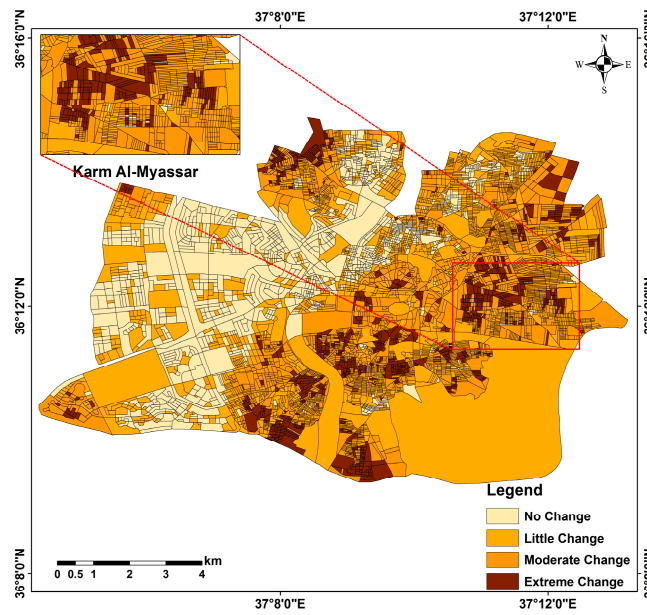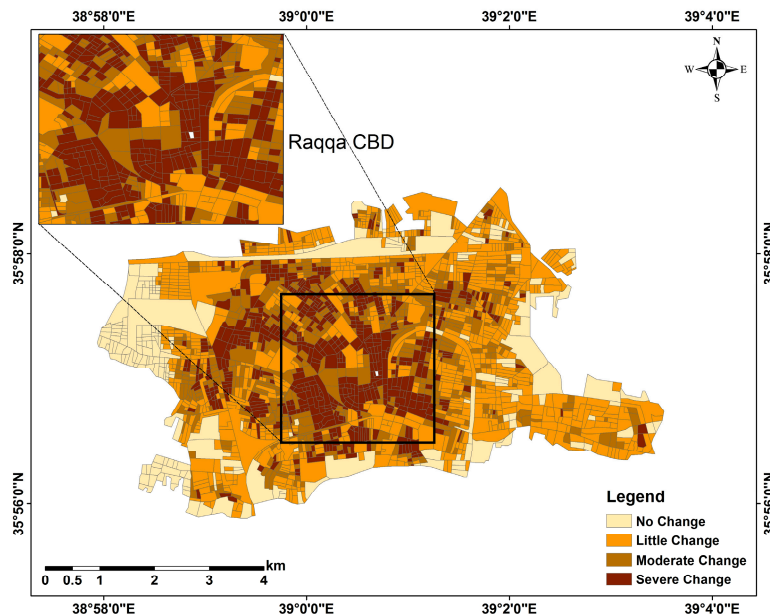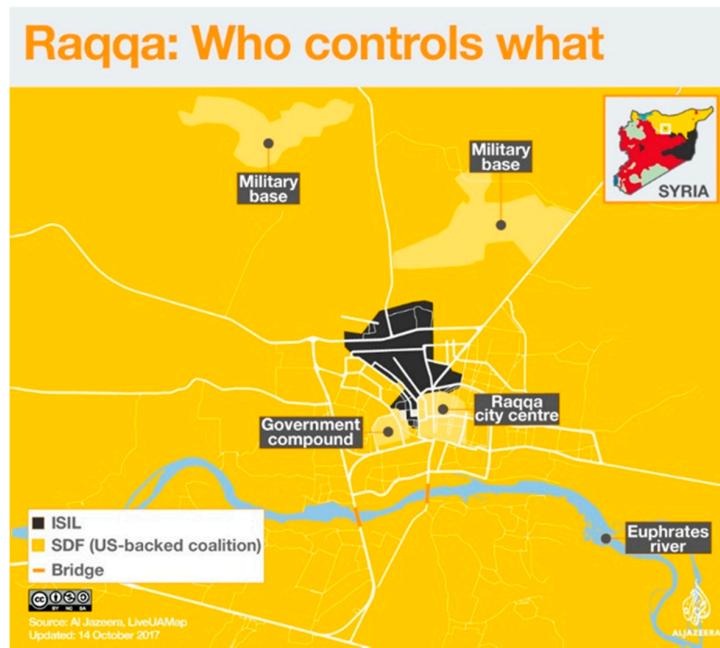
Figure 17. Aleppo standard deviation map shows higher standard deviation on street blocks in the eastern side.

In Raqqa, analysis of the standard deviation map reveals severe change (dark brown) on street blocks in the Central Business District (CBD) (Figure 18a). The high standard deviation may be a result of an offensive assault by the United States backed Syrian Democratic Forces (SDF) [43]. The outskirts of the city, however, have a low standard deviation, hence the street blocks on the fringes of the city experienced less change as compared to the CBD. This was hinted at in maps, indicating how the SDF launched their operation through airstrikes (Figure 18b).
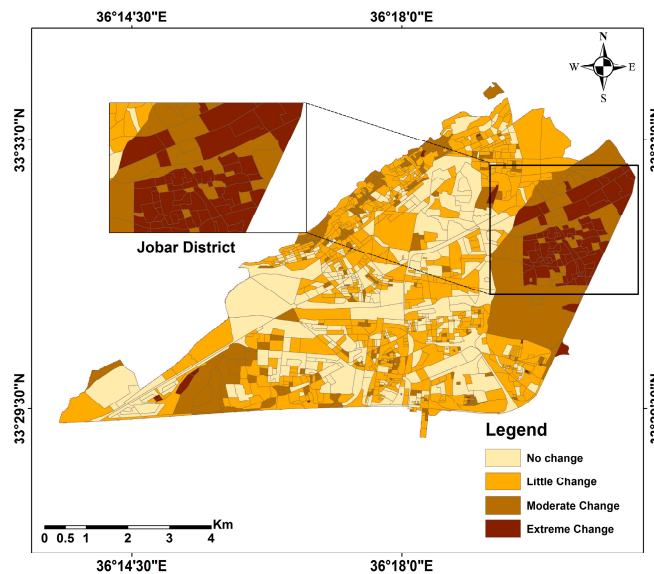

(**a**)

Figure 18. *Cont*.

(**b**)

Figure 18. Comparison of Raqqa standard deviation map (**a**) and territory map (**b**) produced by Aljazeera [43].

The standard deviation map for Damascus shown in Figure 19a generally shows low levels of change for most street blocks in the city. The city has been known to be stable and conflict free for most of the civil war period [48], hence most street blocks in the city reflect this by showing little to no change (light brown color). However, the eastern part seems to show street blocks with a very high standard deviation, signifying an extreme change in the area this may have resulted from destruction from air strikes on the rebel-held Jobar district [49]. The northeastern neighborhoods of Jobar and Abbaisid Square are said to have experienced the most intense fighting [50], as illustrated in Figure 19.
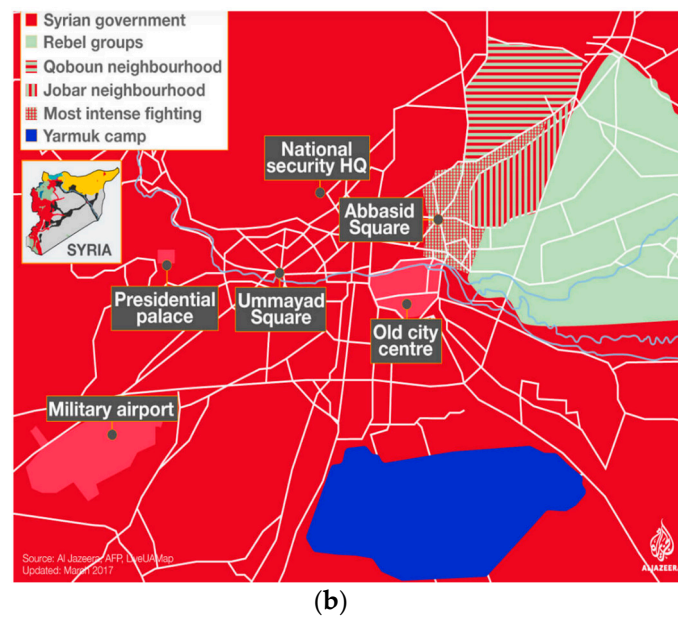

(**a**)

Figure 19. *Cont.*

(**b**)

Figure 19. Comparison of Damascus standard deviation map (**a**) and territory map (**b**) produced by Aljazeera [50].

4. Discussion

Apart from the CCD technique, other SAR techniques have been used for change-detection in disaster situations, for example, damage detection techniques based on time-series SAR imagery [4,51]. These methods make use of amplitude and rely on backscatter information from SAR images; in this case, building damage resulting from disaster occurrences can be detected by comparing the backscatter information exhibited by the pre-disaster and post-disaster images [52]. However, since backscatter information is reliant on the dielectric constant, surface roughness, and the incident angle of an object, coherence information becomes essential to detect damage, especially when the backscattering characteristics remain the same between two images. As we have seen from the results, the coherence value does not rely on the backscattering characteristics of the SAR images but instead the similarity/difference of the phase properties of two SAR images. However, other interferometric SAR techniques have been used for damage detection [53]; in this case, the coherence images obtained by interferometric processing are used for damage detection and assessment, as in this study.

The pre-event and post event results in the experiments show rapid changes that occur between these periods, which is indicated by massive loss of coherence, for example, the city of Raqqa shows an 82.5% loss in coherence that is close to the 80% destruction of the city as reported by the media. The CCD technique thus becomes suitable for detection of such changes. In addition to this, we see from the classification results that coherence images can be divided into different classes based on how each class responds to coherence loss. For example, urban areas exhibit predominantly high coherence and generally experience lower coherence loss over time as compared to vegetation and water bodies. This knowledge can be used for classification of SAR images [54], while it is not possible to use amplitude information alone.

The CCD technique is not new and has been widely employed in various remote sensing applications and highlights the capabilities of Sentinel-1 data. This emerging remote sensing resource provides global coverage and archival data, making it ideally suited to support decision-making tasks during and after disaster events. Despite these benefits, however, the Sentinel-1 mission only started in 2014, and as a result, it does not have an archive of images prior to 2014. This is particularly challenging when monitoring the effects of long-term disasters like wars if the period being investigated

commenced before the mission began. Processing Sentinel-1 data is also time consuming and user intensive, therefore, limiting the applicability of the CCD technique.

In future work, we will develop an automated CCD technique for global background observation using Sentinel-1 imagery. CCD must be automated for use in urban planning, vegetation monitoring, and forest cover management applications if Sentinel-1 is to be fully exploited [54]. Methods for automatic/unsupervised change-detection using SAR data have been proposed in previous studies [33,35]. An Automatic CCD technique can also provide information on areas affected by a disaster. However, coherence matching requires two images acquired with the same looking angle, and thus a 6 to 12-day revisit time of the Sentinel-1 satellites may not be adequate for immediate intervention and response to disasters. With larger constellations, like the COSMO SkyMed constellation, faster revisit times are possible. However, for the quickest possible response times, images are acquired from different angles, rendering our method unusable under such circumstances. Nevertheless, considering the advantages of Sentinel-1 data, new automatic change-detection methods would facilitate the use of CCD in a wider range of contexts.

As seen from the results, temporal coherence is a product created from repeat-pass InSAR observations and, thus, is susceptible to changes in the scene during the two acquisitions. The effects of temporal decorrelation are evident in the time-series coherence images shown in Figures 3–8 and the classification graphs in Figure 9. Decorrelation increases as temporal distances between the slave and master image increase. In this study, a single master image, selected from the middle of the timeline, was co-registered to subsequent slave images, ensuring that the temporal baseline is minimized by distributing decorrelation in both temporal directions and at the same time maintaining the time separation between pre-event and post-event periods.

In vegetated areas like forests, however, this method may not be effective as coherence is highly sensitive to change. Therefore, Coherence Change-Detection (CCD) is not as effective in highly vegetated areas as it is in urban areas [24]. A possible solution to low coherence resulting from temporal decorrelation would be to apply the short baseline approach that separates the master and slave images by short periods, for example, separating the two images by a period of 12 days to a month, so that high coherence is maintained in each coherence image. This, however, is not very useful for analyzing the effects of disaster events over time. Nevertheless, built up areas in urban settings are generally stable over time. Therefore, temporal decorrelation has little effect on the coherence values representing the built-up area. As a result, selecting one single master image is a more appropriate technique in urban areas. Additionally, the comparative results shown in Figure 10 indicate that as compared to vegetated areas, built up areas are affected more by war and earthquakes. Vegetated areas, however, are more affected by hurricanes and fire disasters. The reasons for this may be that during wartime, infrastructure is targeted for destruction. Earthquakes, however, are characterized by shaking of the ground and result in infrastructure instability leading to destruction. Consequently, the CCD technique may be more useful if applied to areas affected by war and earthquakes rather than by fire and hurricane disasters, as it is a more reliable technique for built-up areas.

Although the standard deviation method, applied in the study, reveals areas that have experienced the most change, it is not effective when quantifying the intensity of damage. Furthermore, coherence is affected by small changes in a scene, hence, at times, it is difficult to distinguish small changes from big changes. This is also problematic when selecting an ideal threshold, especially since a variety of factors might be responsible for coherence loss, for example, new built-up areas cannot be distinguished from some vegetated areas [33]. It is essential, therefore, to find methods to improve detection and assessment of the intensity of damage.

5. Conclusions

This study demonstrates the ability of Sentinel-1 C-band imagery to provide information for disaster monitoring and management. Unlike most imaging remote sensing systems, the Sentinel-1 mission provides continuous, reliable global data, which makes it ideal for monitoring any type of

disaster anywhere in the world. Sentinel-1 data from Aleppo, Damascus, and Raqqa in Syria, Sarpol Zahab in Iran, and Puerto Rico, and Santa Rosa CA, USA, were used to generate coherence maps for each of the areas in the periods before, during, and after disasters.

Classifying coherence maps into areas of change and no-change, then applying a threshold of 0.6 and comparing the time series for each period, shows the coherence loss after a particular damaging event. However, differentiating disaster induced coherence loss and temporal coherence loss is not easy on coherence maps; hence, standard deviation analysis was used in combination with street-blocks to identify which street blocks in the areas experienced a sudden loss in coherence, which may be an indication of disaster effects.

Classifying images into built-up, vegetation, bare soil, and water bodies and integrating these land-use classes with the coherence images helped show the effects of coherence loss on each class after each disaster. For future studies, coherence can be used not only as a measure of change in CCD but also for classification, as the study showed that different classes exhibited dissimilar coherence loss over time. Furthermore, future studies will focus on automating the CCD method for global disaster monitoring.

References

1. Huyck, C.; Verrucci, E.; Bevington, J. Remote sensing for disaster response: A rapid, image-based perspective. In *Earthquake Hazard, Risk and Disasters*; Elsevier: Amsterdam, The Netherlands, 2014; pp. 1–24.
2. Ohkura, H.; Jitsufuchi, T.; Matsumoto, T.; Fujinawa, Y. Application of SAR data to monitoring of earthquake disaster. *Adv. Space Res.* **1997**, *19*, 1429–1436. [CrossRef]
3. Dong, Y.; Li, Q.; Dou, A.; Wang, X. Extracting damages caused by the 2008 Ms 8.0 Wenchuan earthquake from SAR remote sensing data. *J. Asian Earth Sci.* **2011**, *40*, 907–914. [CrossRef]
4. Matsuoka, M.; Yamazaki, F. Use of SAR imagery for monitoring areas damaged due to the 2006 Mid Java, Indonesia earthquake. In Proceedings of the 4th International Workshop on Remote Sensing for Post-Disaster Response, Cambridge, UK, 25–26 September 2006.
5. Stramondo, S.; Moro, M.; Tolomei, C.; Cinti, F.; Doumaz, F. InSAR surface displacement field and fault modelling for the 2003 Bam earthquake (southeastern Iran). *J. Geodyn.* **2005**, *40*, 347–353. [CrossRef]
6. Balz, T.; Liao, M. Building damage detection using post-seismic high-resolution SAR satellite data. *Int. J. Remote Sens.* **2010**, *31*, 3369–3391. [CrossRef]
7. Gähler, M. Remote Sensing for Natural or Man-made Disasters and Environmental Changes. *Environ. Appl. Remote Sens.* **2016**, 309–338. [CrossRef]
8. Lu, D.; Mausel, P.; Brondizio, E.; Moran, E. Change detection techniques. *Int. J. Remote Sens.* **2004**, *25*, 2365–2401. [CrossRef]
9. Wang, F.; Xu, Y.J. Comparison of remote sensing change detection techniques for assessing hurricane damage to forests. *Environ. Monit. Assess.* **2010**, *162*, 311–326. [CrossRef] [PubMed]
10. Singh, A. Review article digital change detection techniques using remotely-sensed data. *Int. J. Remote Sens.* **1989**, *10*, 989–1003. [CrossRef]
11. Hoque, M.A.-A.; Phinn, S.; Roelfsema, C.; Childs, I. Tropical cyclone disaster management using remote sensing and spatial analysis: A review. *Int. J. Disaster Risk Reduct.* **2017**, *22*, 345–354. [CrossRef]
12. Ramsey, E., III; Rangoonwala, A.; Middleton, B.; Lu, Z. Satellite optical and radar data used to track wetland forest impact and short-term recovery from Hurricane Katrina. *Wetlands* **2009**, *29*, 66–79. [CrossRef]
13. Li, X.; Yu, L.; Xu, Y.; Yang, J.; Gong, P. Ten years after Hurricane Katrina: Monitoring recovery in New Orleans and the surrounding areas using remote sensing. *Sci. Bull.* **2016**, *61*, 1460–1470. [CrossRef]

14. Rowell, A.; Moore, P.F. *Global Review of Forest Fires*; Citeseer: Forest Grove, OR, USA, 2000.

15. Anggraeni, A.; Lin, C. Application of SAM and SVM Techniques to Burned Area Detection for Landsat TM Images in Forests of South Sumatra. In Proceedings of the International Conference on Environmental Science and Technology, Singapore, 26–28 February 2011; pp. V2160–V2164.

16. Marx, A.J. Detecting urban destruction in Syria: A Landsat-based approach. *Remote Sens. Appl. Soc. Environ.* **2016**, *4*, 30–36. [CrossRef]

17. Woodcock, C.E.; Allen, R.; Anderson, M.; Belward, A.; Bindschadler, R.; Cohen, W.; Gao, F.; Goward, S.N.; Helder, D.; Helmer, E. Free access to Landsat imagery. *Science* **2008**, *320*, 1011–1011. [CrossRef] [PubMed]

18. Liu, C.; Dong, P.; Shi, Y. Recurrence interval of the 2008 Mw 7.9 Wenchuan earthquake inferred from geodynamic modelling stress buildup and release. *J. Geodyn.* **2017**, *110*, 1–11. [CrossRef]

19. CNN, Powerful Iran-Iraq Earthquake Is Deadliest of 2017. Available online: https://edition.cnn.com/2017/11/12/middleeast/iraq-earthquake/index.html (accessed on 27 February 2018).

20. Krassenburg, M. Sentinel-1 mission status. In Proceedings of the 11th European Conference on Synthetic Aperture Radar (EUSAR 2016), Hamburg, Germany, 6–9 June 2016; pp. 1–6.

21. Bamler, R.; Hartl, P. Synthetic aperture radar interferometry. *Inverse Probl.* **1998**, *14*, 53–102. [CrossRef]

22. Woodhouse, I.H. *Introduction to Microwave Remote Sensing*; CRC Press: Boca Raton, FL, USA, 2005.

23. Lusch, D.P. *Introduction to Microwave Remote Sensing*; Center for Remote Sensing and Geographic Information Science Michigan State University: East Lansing, MI, USA, 1999.

24. Jendryke, M.; McClure, S.; Balz, T.; Liao, M. Monitoring the built-up environment of Shanghai on the street-block level using SAR and volunteered geographic information. *Int. J. Digital Earth* **2017**, *10*, 675–686. [CrossRef]

25. Ferrettia, M. *InSAR Principles: Guidelines for SAR Interferometry Processing and Interpretation*; ESTEC: Noordwijk, The Netherlands, 2007.

26. Hagberg, J.O.; Ulander, L.M.; Askne, J. Repeat-pass SAR interferometry over forested terrain. *IEEE Trans. Geosci. Remote Sens.* **1995**, *33*, 331–340. [CrossRef]

27. Li, F.K.; Goldstein, R.M. Studies of multibaseline spaceborne interferometric synthetic aperture radars. *IEEE Trans. Geosci. Remote Sens.* **1990**, *28*, 88–97. [CrossRef]

28. Lopez-Martinez, C.; Fabregas, X.; Pottier, E.; Polarimetrie, E.I.R.-T. In A new alternative for SAR imagery coherence estimation. In Proceedings of the 5th European Conference on Synthetic Aperture Radar (EUSAR'04), Ulm, Germany, 25–27 May 2004.

29. Kampes, B.; Usai, S. In Doris: The delft object-oriented radar interferometric software. In Proceedings of the 2nd International Symposium on Operationalization of Remote Sensing, Enschede, The Netherlands, 16–20 August 1999; p. 20.

30. Prati, C.; Rocca, F. Range resolution enhancement with multiple SAR surveys combination. In Proceedings of the International IEEE Geoscience and Remote Sensing Symposium (IGARSS'92), Houston, TX, USA, 26–29 May 1992; pp. 1576–1578.

31. Bruzzone, L.; Marconcini, M.; Wegmuller, U.; Wiesmann, A. An advanced system for the automatic classification of multitemporal SAR images. *IEEE Trans. Geosci. Remote Sens.* **2004**, *42*, 1321–1334. [CrossRef]

32. Preiss, M.; Stacy, N.J. *Coherent Change Detection: Theoretical Description and Experimental Results*; Defence Science and Technology Organisation Edinburgh: Canberra, Australia, 2006.

33. He, M.; He, X. Urban change detection using coherence and intensity characteristics of multi-temporal SAR imagery. In Proceedings of the 2nd IEEE Asian-Pacific Conference on Synthetic Aperture Radar (APSAR 2009), Xian, China, 26–30 October 2009; pp. 840–843.

34. Jendryke, M.; Balz, T.; McClure, S.C.; Liao, M. Putting people in the picture: Combining big location-based social media data and remote sensing imagery for enhanced contextual urban information in Shanghai. *Comput. Environ. Urban Syst.* **2017**, *62*, 99–112. [CrossRef]

35. Perissin, D.; Wang, Z.Y.; Wang, T. The SarProZ InSAR tool for urban subsidence/manmade structure stabilirt monitoring in China. In Proceedings of the ISRSE, Sidney, Australia, 10–15 April 2011.

36. Mocnik, F.-B.; Zipf, A.; Raifer, M. The OpenStreetMap folksonomy and its evolution. *Geo-Spat. Inf. Sci.* **2017**, *20*, 219–230. [CrossRef]

37. Kafi, K.; Shafri, H.; Shariff, A. An analysis of LULC change detection using remotely sensed data; A Case study of Bauchi City. In *IOP Conference Series: Earth and Environmental Science*; IOP Publishing: Bristol, UK, 2014.

38. LA Times, Santa Rosa Comes to Terms with the Scale of Devastation: 3000 Buildings Lost, Many Dead in Fire. Available online: http://www.latimes.com/local/lanow/la-me-santa-rosa-fire-toll-20171014-story.html (accessed on 15 December 2017).

39. Almasdar News, US-Backed Forces Succeed in Making Raqqa 80 Percent "Uninhabitable". Available online: https://www.almasdarnews.com/article/us-backed-forces-succeed-making-raqqa-80-percent-uninhabitable/ (accessed on 26 October 2017).

40. Reuters, "Strong Earthquake Hits Iraq and Iran, Killing at Least 210". Available online: https://www.reuters.com/article/us-iraq-quake/strong-earthquake-hits-iraq-and-iran-killing-more-than-450-idUSKBN1DC0VZ?il=0 (accessed on 12 November 2017).

41. NY Times, How California's Most Destructive Wildfire Spread, Hour by Hour. Available online: https://www.nytimes.com/interactive/2017/10/21/us/california-fire-damage-map.html (accessed on 3 March 2018).

42. IB Times, The Fall of Aleppo Timeline: How Assad Captured Syria's Biggest City. Available online: http://www.ibtimes.co.uk/fall-aleppo-timeline-how-assad-captured-syrias-biggest-city-1596504 (accessed on 1 November 2017).

43. Reuters, U.S.-Backed Force Launches Assault on Islamic State's 'Capital' in Syria. Available online: https://www.reuters.com/article/us-mideast-crisis-syria-raqqa/u-s-backed-force-launches-assault-on-islamic-states-capital-in-syria-idUSKBN18W29P (accessed on 26 October 2017).

44. Al Jazeera, Fighting Intensifies in Damascus: Rebels Gain Control of Areas Close to Syrian Capital, with Fighting Affecting Operations at International Airport. Available online: https://www.aljazeera.com/news/middleeast/2013/03/2013316133433170554.html (accessed on 6 March 2018).

45. UNITAR, Damaged Structures and Related Density Map in Sarpol-e-Zahab. Available online: http://www.unitar.org/unosat/map/2732 (accessed on 3 March 2018).

46. LA Times, Here's Where More than 7500 Buildings Were Destroyed and Damaged in California's Wine Country Fires. Available online: http://www.latimes.com/projects/la-me-northern-california-fires-structures/ (accessed on 27 February 2018).

47. BBC, Aleppo Battle: Syrian Troops Push Deeper into Rebel-Held East. Available online: http://www.bbc.com/news/world-middle-east-38207231 (accessed on 3 March 2018).

48. Daily Mail, a Tale of Two Cities: How One Side of Damascus Stands Tall BUT the Other Has Been Flattened by Assad in One of the Most Brutal Bombing Campaigns in History. Available online: http://www.dailymail.co.uk/news/article-5456783/A-tale-two-cities-Damascus-brutal-divide.html (accessed on 15 March 2018).

49. Reuters, Syrian Forces and Rebels Fight Fierce Clashes in Northeast Damascus. Available online: https://www.reuters.com/article/us-mideast-crisis-syria-jobar/syrian-forces-and-rebels-fight-fierce-clashes-in-northeast-damascus-idUSKBN16Q09X (accessed on 3 March 2018).

50. The Telegraph, Syrian Rebels Launch Surprise Attack on Damascus. Available online: https://www.telegraph.co.uk/news/2017/03/19/syrian-rebels-launch-surprise-attack-damascus/ (accessed on 3 March 2018).

51. Matsuoka, M.; Yamazaki, F. Use of Interferometric Satellite SAR for Earthquake Damage Detection. In Proceedings of the 6th International Conference on Seismic Zonation, Palm Springs, CA, USA, 12–15 November 2000; EERI: Oakland, CA, USA, 2000.

52. Dong, L.; Shan, J. A comprehensive review of earthquake-induced building damage detection with remote sensing techniques. *ISPRS J. Photogramm. Remote Sens.* **2013**, *84*, 85–99. [CrossRef]

53. Papathanassiou, K.P.; Cloude, S.R. Single-baseline polarimetric SAR interferometry. *IEEE Trans. Geosci. Remote Sens.* **2001**, *39*, 2352–2363. [CrossRef]

54. Santoro, M.; Shvidenko, A.; McCallum, I.; Askne, J.; Schmullius, C. Properties of ERS-1/2 coherence in the Siberian boreal forest and implications for stem volume retrieval. *Remote Sens. Environ.* **2007**, *106*, 154–172. [CrossRef]